J Mater Sci (2020) 55:116–124

Chemical routes to materials

Flexible tuning of hole-based localized surface plasmon resonance in roxbyite $Cu_{1.8}S$ nanodisks via particle size, carrier density and plasmon coupling

Lihui Chen[1,*], Haifeng Hu[1], Yuan Li[1], Rui Chen[1], and Guohua Li[1,2,*]

[1] College of Chemical Engineering, Zhejiang University of Technology, 18, Chaowang Road, Hangzhou 310014, China
[2] State Key Breeding Base of Green Chemistry Synthesis Technology, Zhejiang University of Technology, 18, Chaowang Road, Hangzhou 310032, China

Received: 11 June 2019
Accepted: 10 August 2019
Published online: 21 August 2019

ABSTRACT

Semiconductor nanocrystals (NCs) heavily doped with cation/anion vacancies or foreign metal ions can support localized surface plasmon resonance (LSPR) in the near-infrared (NIR) and mid-infrared (MIR) spectral wavelengths. Typically, nonstoichiometric copper sulfide $Cu_{2-x}S$ NCs with different x values ($0 < x \leq 1$) have attracted numerous attention because of hole-based, particle size, morphology, hole density and crystal phase-dependent LSPR. In spite of excited development of methodology for LSPR manipulation, systematic LSPR tuning of $Cu_{2-x}S$ NCs with a special crystal phase has been limited. Herein, roxbyite $Cu_{1.8}S$ nanodisks (NDs) were selected as a model and their LSPR was readily tuned by particle size, hole density via chemical oxidation and reduction, self-assembly and disassembly in solution and plasmon coupling in multilayer films. Particle size, hole density and plasmon coupling severely affect their LSPR peak position and absorption intensity. Therefore, the ability of flexible LSPR tuning gifts roxbyite $Cu_{1.8}S$ NDs great potential in plasmonic applications, including photocatalysis, photothermal agent, two-photon photochemistry and many others in NIR and MIR regions.

Introduction

Copper sulfide $Cu_{2-x}S$ nanocrystals (NCs) degenerately doped with copper vacancy, exhibit localized surface plasmon resonance (LSPR) because of the collective oscillation of free holes with incident light [1–3]. Because of the much lower carrier (hole) density ($N_h \approx 10^{20}$–10^{21} cm^{-3}) compared with noble metals ($N_e \approx 10^{23}$ cm^{-3}), the $Cu_{2-x}S$ NCs exhibit LSPR responses in near-infrared (NIR) and mid-infrared (MIR) regions [4]. Unlike plasmonic metal such as Cu, Ag and Au with face-centered cubic (fcc) crystal phase, $Cu_{2-x}S$ possesses a variety of crystal

Address correspondence to E-mail: lihuichen@zjut.edu.cn; nanozjut@zjut.edu.cn

https://doi.org/10.1007/s10853-019-03923-9

phases varying from copper-abundant chalcocite Cu_2S, djurleite $Cu_{1.94}S$, roxbyite and digenite $Cu_{1.8}S$ to copper-poor covellite CuS phase [5]. $Cu_{2-x}S$ NCs with different crystal phases exhibit distinct LSPR response, for instance djurleite $Cu_{1.94}S$ nanodisks (NDs) have two broad LSPR peaks in NIR and MIR regions, while covellite CuS NDs have only one narrow peak in NIR region [6, 7]. Due to the unique crystal phase-dependent LSPR properties, djurleite $Cu_{1.94}S$ was applied for cathodes in all-vanadium redox flow batteries, and covellite CuS was utilized as a photothermal agent and an electron donor to promote the photocatalytic water splitting efficiency of TiO_2 [8–10].

In addition to the factor of crystal phase, the LSPR properties of $Cu_{2-x}S$ NCs could be finely manipulated by particle size, morphology, hole density, as well as plasmon coupling [11–14]. In chalcocite Cu_2S/$Cu_{2-x}S$ NDs, the LSPR peak position was tuned by ND size. The out-of-plane oscillation peak blue-shifted with increasing size, while the in-plane oscillation peak red-shifted [11]. Besides particle size, the LSPR peak position and intensity were adjusted by morphology in chalcocite Cu_2S/$Cu_{2-x}S$ nanospheres (NSs) and nanorods (NRs) [12]. Furthermore, in chalcocite Cu_2S NSs, the hole density was increased by iodine oxidation and decreased by decamethylcobaltocene reduction, respectively. Hole density severely affected the LSPR peak position, absorption intensity and peak width of chalcocite Cu_2S NSs [13]. In assembled thin films, covellite CuS NDs exhibited much stronger plasmon coupling effect than that of chalcocite Cu_2S NDs and digenite $Cu_{1.8}S$ NDs [14]. However, previous researches mainly focused on the LSPR tuning of chalcocite Cu_2S phase, and research on other crystal phases has been rarely demonstrated. On account of crystal phase not only determine the hole density and copper ion mobility, but also the hole distribution in the sulfur lattices. The aforementioned tuning approaches for chalcocite Cu_2S could not be simply applied to other crystal phases, since the influence factors of LSPR were correlated with each other. Therefore, systematic investigation on LSPR tuning of $Cu_{2-x}S$ NCs with a special crystal phase instead of the chalcocite Cu_2S is fundamentally interesting.

We selected roxbyite $Cu_{1.8}S$ with moderate hole density as a model and systematically tuned their LSPR. Such investigation could provide deeper understanding of crystal phase-dependent LSPR and further development of potential applications of roxbyite $Cu_{1.8}S$. Herein, uniform $Cu_{1.8}S$ NDs were wet-chemically synthesized and their LSPR properties such as peak position, absorption intensity and peak width were flexibly tuned. Particle size, hole density via chemical oxidation and reduction, self-assembly and disassembly in solution, as well as plasmon coupling in solid film, severely affected the LSPR of $Cu_{1.8}S$ NDs. Therefore, the large tunability of LSPR suggests roxbyite $Cu_{1.8}S$ ND is a potential candidate for plasmonic photocatalysis, photothermal therapy, two-photon photochemistry and many others in NIR region.

Experimental details

Synthesis of $Cu_{1.8}S$ nanodisks (NDs) with roxbyite phase

The synthesis of roxbyite $Cu_{1.8}S$ NDs was modified from a previous report [15]. Typically, 1.5 mmol of copper (II) stearate, 4.0 mmol of *N*,*N*-dibutylthiourea (DBTU) and 3.0 mL of oleylamine (as reducing agent, ligand and solvent) were added in a 100-mL test tube and heated at 80 °C at the rate of 5 °C/min under N_2 atmosphere. After further stirring at 80 °C for 15 min, 30 min and 60 min, the mixture was cooled to room temperature and purified with toluene and ethanol by centrifugation and finally dispersed in toluene and/or chloroform ($CHCl_3$). The prepared samples were stored in the glovebox for further characterizations.

Characterizations

TEM observations were carried out using a JEM-1011 transmission electron microscope (JEOL) at an accelerating voltage of 100 kV. SEM observations were carried out using an S-4800 (HITACHI) Field-Emission Scanning Electron Microscope (FE-SEM) at an accelerating voltage of 5 kV. UV–Vis–NIR (300–2500 nm) absorption spectra of individual and coupled $Cu_{1.8}S$ NDs and corresponding multilayer films were measured using U-4100 spectrophotometer (HITACHI). The XRD patterns were taken on X'Pert Pro MPD (PANalytical) with CuKα radiation (λ = 1.542 Å) at 45 kV and 40 mA. In order to exclude the air oxidation effect on the samples, the XRD measurement should be carried out in inert

atmosphere. Briefly, the samples deposited on the substrate were dried in glovebox and transported to N_2-blanketed XRD holder for measurement immediately.

Results and discussion

Tuning of LSPR by particle size

An organic sulfur source DBTU was utilized to synthesize uniform roxbyite $Cu_{1.8}S$ NCs. Figure 1a–c shows the prepared hexagonal disk-shaped NCs at the reaction time of 15 min, 30 min and 60 min. The diameter of the nanodisks (NDs) varied from 9.3 to 13.4 nm and to 14.9 nm, while the thickness varied from 3.3 to 3.8 nm and to 4.0 nm. The larger increment in diameter demonstrates that the NDs were tightly enclosed by oleylamine (OAm) molecules in basal crystal planes which resulted in faster deposition of copper and sulfur species along the lateral directions. The OAm-capped NDs individually dispersed in toluene and chloroform ($CHCl_3$), and no coupled ND assemblies were observed. The copper vacancies (free holes) in the $Cu_{1.8}S$ ND collectively oscillate with incident light which led to a broad and intense absorption in NIR region (Fig. 1d) [15]. Because of a retardation effect caused by uneven electric field across the particle, the LSPR peak of $Cu_{1.8}S$ NDs red-shifts from 1500 nm to 1660 nm and to 1706 nm with increasing aspect ratio [16, 17]. The growth of roxbyite $Cu_{1.8}S$ with reaction time did not decrease the hole density, which was derived from the case of digenite $Cu_{2-x}S$ NCs [18]. Large variation in LSPR response tuned by particle size suggests the $Cu_{1.8}S$ NDs are capable of size-dependent plasmonic applications such as photothermal therapy and photocatalytic organic synthesis [19, 20]. Noticeably, roxbyite $Cu_{1.8}S$ NDs exhibit single LSPR peak which is different from djurleite $Cu_{1.94}S$ and digenite $Cu_{1.8}S$ NDs with two distinct LSPR peaks [14]. The singular LSPR peak in roxbyite $Cu_{1.8}S$ NDs mainly originates from in-plane oscillation mode, resulting in enhanced electric field distribution at sharp corners of the ND (Fig. 1e) [21, 22].

Tuning of LSPR by hole density via chemical oxidation and reduction

In addition to particle size, the LSPR of roxbyite $Cu_{1.8}S$ NDs was tuned by air-induced oxidation and 3-mercaptopropionic acid (MPA)-induced reduction. The freshly prepared, a certain amount of $Cu_{1.8}S$ NDs were dispersed in 5.0 mL toluene and then exposed to air with magnetic stirring. Time evolution of LSPR absorptions was recorded afterward (Fig. 2a). The LSPR peak gradually blue-shifted, and the absorption intensity increased with oxidation time. This variation of LSPR can be ascribed to an increase in hole density, which has been well investigated in $Cu_{2-x}Se$ NCs [23]. Oxygen extracted Cu^+ in the crystal lattice of roxbyite $Cu_{1.8}S$ and oxidized the Cu^+ into Cu^{2+}

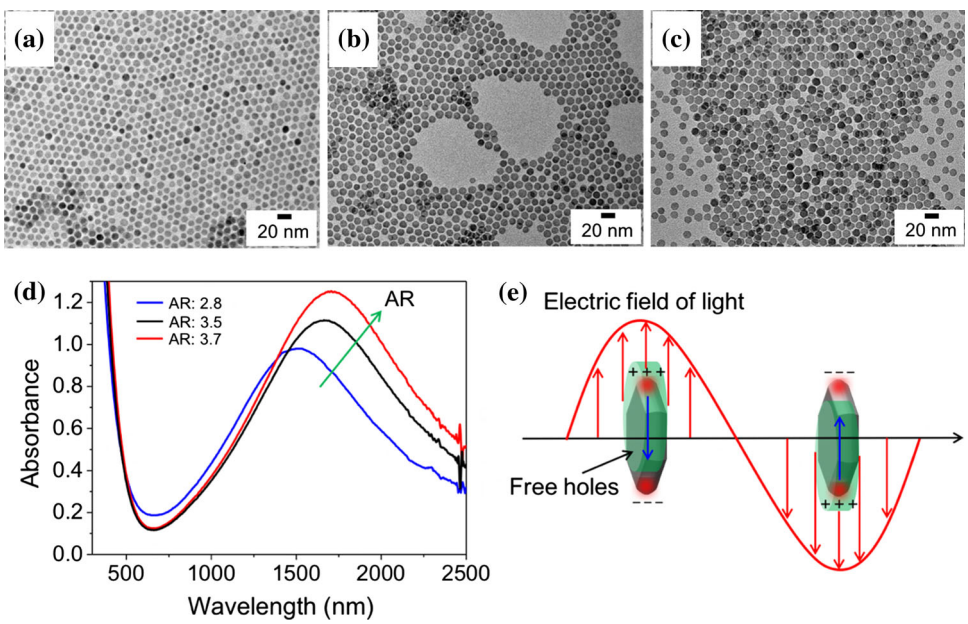

Figure 1 TEM images of prepared roxbyite $Cu_{1.8}S$ NDs by control of the reaction time at **a** 15 min, **b** 30 min and **c** 60 min. **d** UV–Vis–NIR absorption spectra of $Cu_{1.8}S$ NDs with different aspect ratios (aspect ratio = AR: diameter/thickness). **e** Scheme of in-plane collective oscillation of free holes with incident light. Blue arrow: anti-electric field in the ND. Red region at corners of ND: enhanced electric field induced by LSPR.

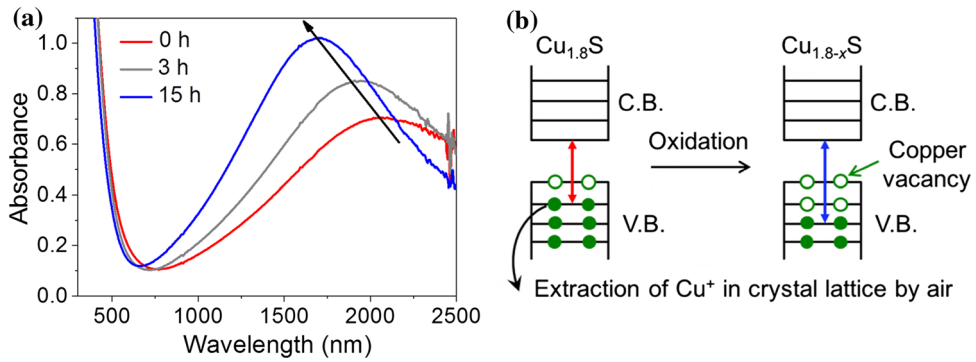

Figure 2 **a** Time evolution of UV–Vis–NIR absorption spectra of roxbyite $Cu_{1.8}S$ NDs under air oxidation. **b** Scheme of air oxidation-induced copper vacancy generation and band gap variation in $Cu_{1.8}S$ ND. *C.B.* conduction band, *V.B.* valence band. Red and blue double-headed arrow: band gap of $Cu_{1.8}S$ ND before and after air oxidation, respectively.

species. Recently, Kaseman et al. reported the air-induced oxidation of OAm-capped $Cu_{2-x}Se$ NCs. Two distinct Cu^{2+} surface species assigned to Cu^{2+} bound to OAm (Cu^{2+}–OAm) and Cu^{2+} located in CuO domain were identified [24]. It is likely that the present OAm-capped roxbyite $Cu_{1.8}S$ NDs experienced similar Cu^{+}/Cu^{2+} transformation under air oxidation. The ND size before and after air oxidation is almost same. A decrease in particle size leads to a blueshifted LSPR peak as well as weakened absorption intensity. In addition, an increase in hole density leads to a blueshifted LSPR peak but enhanced absorption intensity [25]. Therefore, the variation of LSPR response under air oxidation is caused by an increase in hole density rather than a decrease in particle size. The hole density varied from $N_{h1} = 4.47 \times 10^{21}$ cm^{-3} to $N_{h2} = 5.88 \times 10^{21}$ cm^{-3} upon air-induced oxidation. The details of hole density calculation are shown in the supplementary information. Besides LSPR variation, the band gap of $Cu_{1.8}S$ NDs slightly increased possibly due to a Moss–Burstein effect (Fig. 2b) [26]. Tunable hole density of $Cu_{1.8}S$ NDs by simple oxidation is a unique property beyond plasmonic metals. Because of the intense absorption in NIR wavelengths, the oxidized $Cu_{1.8}S$ NDs were applied as a plasmonic sensor. The sensitivity factor was estimated to be 558 nm/RIU (Fig. S1), which is much larger than that of gold nanoparticles in visible wavelengths [27].

Afterward, the oxidized roxbyite $Cu_{1.8}S$ NDs dispersed in 5.0 mL toluene were treated with 5.0 μL of MPA by shaking with hand under N_2 atmosphere (Fig. 3a). The amphiphilic MPA molecules were generally utilized in ligand exchange with the hydrophobic –SH group tightly capping the metal sulfide NC surface, while the hydrophilic –COOH group gifting the NC favorable dispersity in aqueous solutions [28]. In the present study, the proton in –SH group provides MPA reducing ability to fill the copper vacancies in the crystal lattice of roxbyite $Cu_{1.8}S$. The LSPR peak gradually red-shifted, and the absorption intensity decreased with reduction time. This variation of LSPR is due to a decrease in hole density ($N_{h3} = 5.20 \times 10^{21}$ cm^{-3} after MPA reduction), which has been demonstrated in $Cu_{2-x}Se$ NCs [23]. The decrease in hole density arising from the pinning effect near the ND surface by MPA molecules was excluded. It is suggested that the MPA molecules reduced surface Cu^{2+} species of the $Cu_{1.8}S$ ND through the formation of disulfide and/or coordination of MPA to surface copper ions [29, 30]. The reduced copper species filled the holes in the valence band of $Cu_{1.8}S$, and the band gap was slightly decreased (Fig. 3b).

It is noticeable that MPA reduction also resulted in copper and sulfur atoms at the sharp corners of hexagonal ND migrating to inner crystal lattices of $Cu_{1.8}S$ and thus the morphology evolution to rounded plates (Fig. 3c). This observation was similar to a previous report which showed the removal of sulfur and Cu atoms moving to new lattice positions in covellite CuS, leading to the crystal phase and morphology evolution after 1-dodecanethiol (1-DDT) treatment [31]. The air-induced extraction of Cu^{+} in the crystal lattice and MPA-induced reductive filling of holes were confirmed by XRD measurement (Fig. 3d). Air oxidation of freshly synthesized roxbyite $Cu_{1.8}S$ NDs caused a slight shift of $(00\bar{8})$ peak to higher diffraction angle, while the subsequent MPA reduction recovered the diffraction angle. According

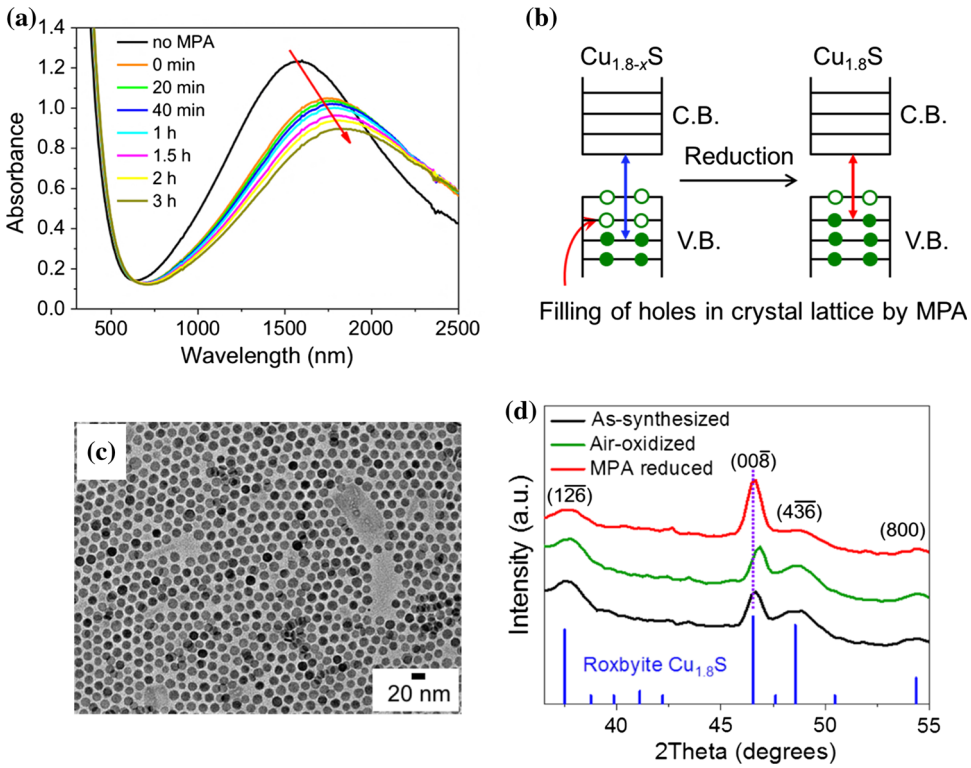

Figure 3 **a** Time evolution of UV–Vis–NIR absorption spectra of roxbyite $Cu_{1.8}S$ NDs under MPA reduction. **b** Scheme of MPA reduction-induced hole filling and band gap variation in $Cu_{1.8}S$ ND. *C.B.* conduction band, *V.B.* valence band. Red and blue double-headed arrow: band gap of $Cu_{1.8}S$ ND before and after MPA reduction, respectively. **c** TEM image of MPA-reduced $Cu_{1.8}S$ NDs. **d** XRD patterns of as-synthesized, air oxidized and MPA-reduced $Cu_{1.8}S$ NDs.

to the Bragg equation, an increase in diffraction angle suggests the lattice contraction of the $Cu_{1.8}S$ ND, which resulted from the extraction of Cu^+ induced by air. On the contrary, a decrease in diffraction angle means the lattice expansion of the $Cu_{1.8}S$ ND, which resulted from the filling of holes or insertion of coppers induced by MPA. Furthermore, the obvious shift of (00$\bar{8}$) diffraction peak in XRD pattern implies higher mobility of Cu^+ in (00$\bar{8}$) crystal plane than that in other crystal planes such as (1$\bar{2}$6), (4 $\bar{3}$6) and (800) in the roxbyite $Cu_{1.8}S$. The variation of LSPR response by air-induced oxidation and MPA-induced reduction were ceased after a period of time (Fig. S2). This "LSPR fixing effect" is consistent with a previous report [32]. In addition to LSPR response, the XRD peak shift of $Cu_{1.8}S$ NDs was also ceased after the completion of oxidation and reduction process (Fig. S3).

Tuning of LSPR by self-assembly and disassembly in solution

Plasmon coupling is an effect caused by the Coulomb interaction between adjacent NCs in an assembly, which induces large variation of LSPR spectrum, intensity, as well as the local electric field spatial distribution, and polarization [33, 34]. Therefore, this effect provides a facile approach to tune the plasmonic properties of metals and semiconductors. In order to trigger the self-assembly, a certain amount of roxbyite $Cu_{1.8}S$ NDs dispersed in 5.0 mL $CHCl_3$ were sonicated with 5.0 μL of MPA under N_2 atmosphere. The LSPR peak of $Cu_{1.8}S$ NDs red-shifted from 1596 to 1682 nm, and the absorption intensity increased after MPA treatment (Fig. 4a). This variation of LSPR response was derived from a shoulder-to-shoulder self-assembly of $Cu_{1.8}S$ NDs (Fig. 4c). The interparticle distance changed from 2.4 nm (Fig. 1c) to 1.5 nm by MPA treatment, and thus, a strong shoulder-to-shoulder in-plane plasmon coupling effect was expected. This fashion of self-assembly occurred probably due to the hydrogen bond between two –COOH groups of the MPA molecules capped on the shoulders of the $Cu_{1.8}S$ ND.

In addition to MPA, the $Cu_{1.8}S$ NDs were also sonicated with 5.0 μL of 1-DDT under N_2 atmosphere. On the contrary, the LSPR peak of $Cu_{1.8}S$ NDs blue-shifted from 1702 to 1460 nm and the absorption intensity dramatically decreased (Fig. 4b). This variation of LSPR response was due to the face-to-face self-assembly of $Cu_{1.8}S$ NDs (Fig. 4d), which was caused by the hydrophobic interactions provided by

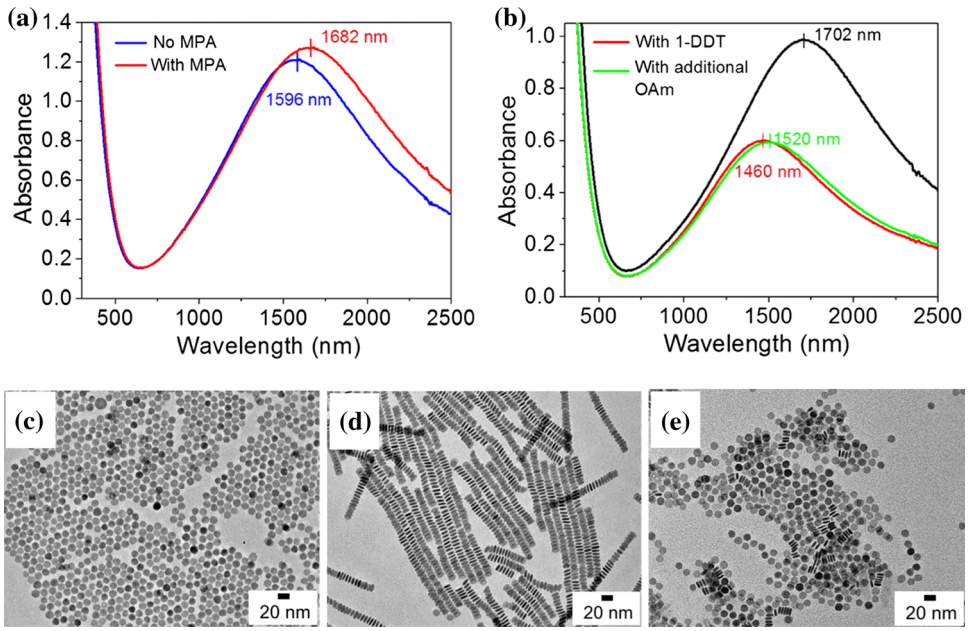

Figure 4 UV–Vis–NIR absorption spectra of roxbyite $Cu_{1.8}S$ NDs treated with **a** MPA, **b** 1-DDT and **c** additional OAm. TEM images of **c** shoulder-to-shoulder assembled $Cu_{1.8}S$ NDs, **d** face-to-face assembled $Cu_{1.8}S$ NDs and **e** disassembled $Cu_{1.8}S$ NDs.

1-DDT molecules (ligand exchange from OAm to 1-DDT) on the basal ND surface [35]. The interparticle distance in the disk array was around 2.1 nm after 1-DDT treatment, and thus, a face-to-face in-plane plasmon coupling effect was expected. The interparticle distance was adjusted by linear thiols with different hydrocarbon chain lengths such as 1-hexanethiol and 1-hexadecanethiol. Besides the plasmon coupling, the dramatic decrease in absorption intensity was caused by the precipitation of long $Cu_{1.8}S$ ND arrays. Afterward, the face-to-face assembled $Cu_{1.8}S$ NDs were disassembled by sonication with 5.0 μL of OAm. The LSPR peak slightly red-shifted from 1460 to 1520 nm, and most of disk arrays were separated (Fig. 3b, e). It is likely that the 1-DDT molecules on the ND surface were replaced by OAm and the nonlinear OAm caused the separation of disk arrays. This observation was consistent with a previous report which demonstrated the ligand exchange from 1-DDT to OAm, leading to the disassembly of supercrystal structures of $Cu_{1.97}S$ NCs [36]. Hence, organic capping ligand triggered self-assembly and disassembly of $Cu_{1.8}S$ NDs is a facile route to tune their LSPR properties. The treatment of roxbyite $Cu_{1.8}S$ NDs with MPA, 1-DDT and OAm did not cause the shift of XRD peak, but it altered the relative peak intensity because of different orientations of NDs on the substrate.

Tuning of LSPR by plasmon coupling in multilayer films

Plasmon coupling of roxbyite $Cu_{1.8}S$ NDs not only emerge in solution, but also in the multilayer films. In order to tune the LSPR of $Cu_{1.8}S$ NDs, two films of $Cu_{1.8}S$ ND and $Cu_{1.8}S$ ND array were assembled through dip coating method. Dip coating was repeated several times to obtain the desired films. Because of uniform size and morphology, the $Cu_{1.8}S$ NDs formed intimately interconnected films with small portion of vacancies (Fig. 5a). Differently, $Cu_{1.8}S$ ND arrays randomly oriented on the substrate (Fig. 5b). It should be noted that the variation of dielectric environment of NDs and ND arrays in the film affected the LSPR of $Cu_{1.8}S$. Indeed, $Cu_{1.8}S$ ND and $Cu_{1.8}S$ ND array films exhibited redshifted and broadened LSPR peak compared to that of colloidal dispersions in $CHCl_3$. The LSPR peak of $Cu_{1.8}S$ ND red-shifted from 1688 nm in colloidal dispersion to 1752 nm in multilayer film (Fig. 5c). The slight redshift can be attributed to an increase in dielectric constant of surrounding medium and a weak in-plane plasmon coupling. Diversely, the LSPR of $Cu_{1.8}S$ ND array red-shifted from 1528 nm in colloidal dispersion to 1920 nm in multilayer film (Fig. 5d). In addition to the increase in dielectric constant of surrounding medium, the large redshift of LSPR peak mainly resulted from a strong in-plane plasmon coupling. This was consistent with a previous report

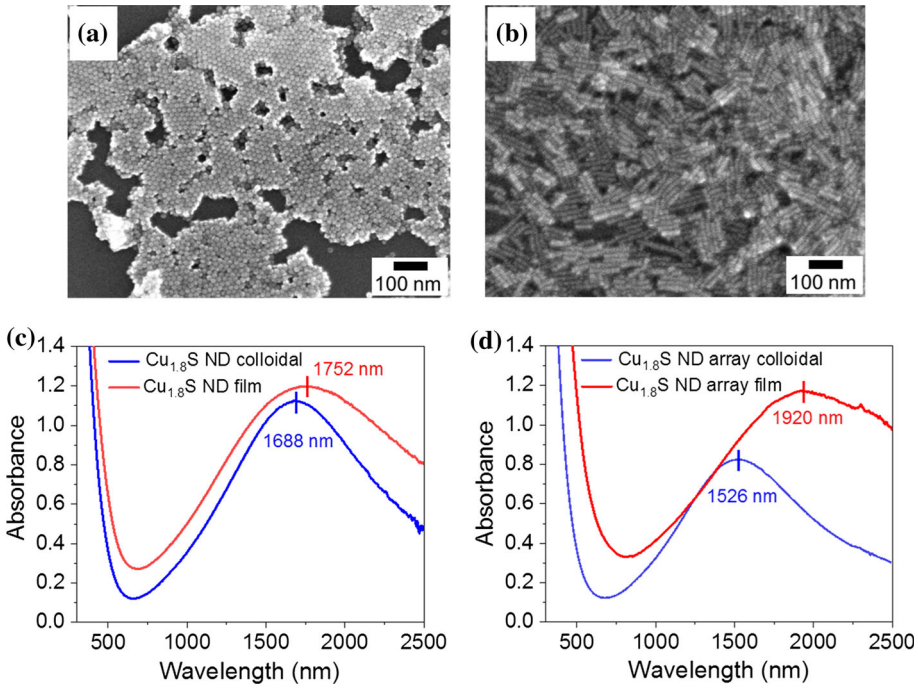

Figure 5 SEM images of multilayer films assembled from **a** individual $Cu_{1.8}S$ NDs and **b** $Cu_{1.8}S$ ND arrays. UV–Vis–NIR absorption spectra of **c** $Cu_{1.8}S$ ND colloidal dispersion and multilayer film and **d** $Cu_{1.8}S$ ND array colloidal dispersion and multilayer film.

concerning covellite CuS NDs [14]. The strong plasmon coupling may lead to an intense electric field on the surface of $Cu_{1.8}S$ ND array film, which is desired to promote two-photon absorption of laser dye and then the subsequent estimation of electric field enhancement factor by hole-based LSPR of $Cu_{1.8}S$ NDs [37].

Conclusions

In summary, high-quality roxbyite $Cu_{1.8}S$ NDs were synthesized and their LSPR were readily tuned by particle size, hole density via chemical oxidation and reduction, self-assembly and disassembly in solution and plasmon coupling in multilayer film. Firstly, the LSPR peak of $Cu_{1.8}S$ NDs red-shifted with increasing particle size. Secondly, the LSPR peak blue-shifted and became stronger and sharper under air oxidation, while it red-shifted and became weaker and wider under MPA reduction. Thirdly, during self-assembly induced by MPA and 1-DDT in $CHCl_3$, the LSPR peak of $Cu_{1.8}S$ NDs red-shifted and became stronger in shoulder-to-shoulder fashion of plasmon coupling, while it blue-shifted and became weaker in face-to-face fashion, respectively. Furthermore, in the disassembly of $Cu_{1.8}S$ ND arrays, the LSPR peak slightly red-shifted. Finally, the plasmon coupling effect occurred in both $Cu_{1.8}S$ ND and $Cu_{1.8}S$ ND array multilayer films, which resulted in a redshift and broadening of LSPR peak. This coupling effect was more significant in $Cu_{1.8}S$ ND array film than that of $Cu_{1.8}S$ ND film. The flexible tunability of LSPR in roxbyite $Cu_{1.8}S$ NDs guarantees potential plasmonic applications in photocatalysis, photothermal therapy, two-photon photochemistry and many others in NIR spectral wavelengths.

Acknowledgements

This work was supported by the Natural Science Foundation of Zhejiang Province (No. LQ19B010002).

Compliance with ethical standards

Conflict of interest The authors declare that they have no conflict of interest.

Electronic supplementary material: The online version of this article (https://doi.org/10.1007/s10853-019-03923-9) contains supplementary material, which is available to authorized users.

References

[1] Kriegel I, Jiang C, Rodríguez-Fernández J, Schaller RD, Talapin DV, da Como E, Feldmann J (2012) Tuning the

excitonic and plasmonic properties of copper chalcogenide nanocrystals. J Am Chem Soc 134:1583–1590

[2] Guo LM, Cao JQ, Zhang JM, Hao YN, Bi K (2019) Photoelectrochemical CO_2 reduction by Cu_2O/Cu_2S hybrid catalyst immobilized in TiO_2 nanocavity arrays. J Mater Sci 54:10379–10388. https://doi.org/10.1007/s10853-019-03615-4

[3] Guillén C, Herrero J (2017) Nanocrystalline copper sulfide and copper selenide thin films with p-type metallic behavior. J Mater Sci 52:13886–13896. https://doi.org/10.1007/s10853-017-1489-4

[4] Luther JM, Jain PK, Ewers T, Alivisatos AP (2011) Localized surface plasmon resonances arising from free carriers in doped quantum dots. Nat Mater 10:361–366

[5] Chakrabarti DJ, Laughlin DE (1983) The Cu–S (copper–sulfur) system. Bull Alloy Phase Diagr 4:254–271

[6] Hsu SW, On K, Tao AR (2011) Localized surface plasmon resonances of anisotropic semiconductor nanocrystals. J Am Chem Soc 133:19072–19075

[7] Xie Y, Carbone L, Nobile C, Grillo V, D'Agostino S, Sala FD, Giannini C, Altamura D, Oelsner C, Kryschi C, Cozzoli PD (2013) Metallic-like stoichiometric copper sulfide nanocrystals: phase- and shape-selective synthesis, near-infrared surface plasmon resonance properties, and their modeling. ACS Nano 7:7352–7369

[8] Li WH, Shavel A, Guzman R, Rubio-Garcia J, Flox C, Fan JD, Cadavid D, Ibaáñez M, Arbiol J, Morante JR, Cabot A (2011) Morphology evolution of $Cu_{2-x}S$ nanoparticles: from spheres to dodecahedrons. Chem Commun 47:10332–10334

[9] Fang JF, Zhang PC, Zhou G (2017) Hydrothermal synthesis of highly stable copper sulfide nanorods for efficient photothermal conversion. Mater Lett 217:71–74

[10] Chandra M, Bhunia K, Pradhan D (2018) Controlled synthesis of CuS/TiO_2 heterostructured nanocomposites for enhanced photocatalytic hydrogen generation through water splitting. Inorg Chem 57:4524–4533

[11] Hsu SW, Bryks W, Tao AR (2012) Effects of carrier density and shape on the localized surface plasmon resonances of $Cu_{2-x}S$ Nanodisks. Chem Mater 24:3765–3771

[12] Kriegel I, Rodríguez-Fernández J, Wisnet A, Zhang H, Waurisch C, Eychmüller A, Dubavik A, Govorov AO, Feldmann J (2013) Shedding light on vacancy-doped copper chalcogenides: shape-controlled synthesis, optical properties, and modeling of copper telluride nanocrystals with near-infrared plasmon resonances. ACS Nano 7:4367–4377

[13] Hartstein KH, Brozek CK, Hinterding SOM, Gamelin DR (2018) Copper-coupled electron transfer in colloidal plasmonic copper-sulfide nanocrystals probed by in situ spectroelectrochemistry. J Am Chem Soc 140:3434–3442

[14] Hsu SW, Ngo C, Tao AR (2014) Tunable and directional plasmonic coupling within semiconductor nanodisk assemblies. Nano Lett 14:2372–2380

[15] Kanehara M, Arakawa H, Honda T, Saruyama M, Teranishi T (2012) Large-scale synthesis of high-quality metal sulfide semiconductor quantum dots with tunable surface-plasmon resonance frequencies. Chem Eur J 18:9230–9238

[16] van de Hulst HC (1981) Light scattering by small particles. Dover, New York

[17] Bohren CF, Huffman DR (1983) Absorption and scattering of light by small particles. Wiley, New York

[18] Zhou DL, Liu D, Xu W, Yin Z, Chen X, Zhou PW, Cui SB, Chen ZG, Song HW (2016) Observation of considerable upconversion enhancement induced by $Cu_{2-x}S$ plasmon nanoparticles. ACS Nano 10:5169–5179

[19] Ding XG, Liow CH, Zhang MG, Huang RJ, Li CY, Shen H, Liu MY, Zou Y, Gao N, Zhang ZJ, Li YG, Wang QB, Li SZ, Jiang J (2014) Surface plasmon resonance enhanced light absorption and photothermal therapy in the second near-infrared window. J Am Chem Soc 136:15684–15693

[20] Cui JB, Li YJ, Liu L, Chen L, Xu J, Ma JW, Fang G, Zhu EB, Wu H, Zhao LX, Wang LY, Huang Y (2015) Near-infrared plasmonic-enhanced solar energy harvest for highly efficient photocatalytic reactions. Nano Lett 15:6295–6301

[21] Chen LH, Sakamoto M, Sato R, Teranishi T (2015) Determination of a localized surface plasmon resonance mode of Cu_7S_4 nanodisks by plasmon coupling. Faraday Discuss 181:355–364

[22] Zhai Y, Shim M (2017) Effects of copper precursor reactivity on the shape and phase of copper sulfide nanocrystals. Chem Mater 29:2390–2397

[23] Dorfs D, Härtling T, Miszta K, Bigall NC, Kim MR, Genovese A, Falqui A, Povia M, Manna L (2011) Reversible tunability of the near-infrared valence band plasmon resonance in $Cu_{2-x}Se$ nanocrystals. J Am Chem Soc 133:11175–11180

[24] Kaseman DC, Jarvi AG, Gan XY, Saxena S, Millstone JE (2018) Evolution of surface copper(II) environments in $Cu_{2-x}Se$ nanoparticles. Chem Mater 30:7313–7321

[25] Zhao YX, Pan HC, Lou YB, Qiu XF, Zhu JJ, Burda C (2009) Plasmonic $Cu_{2-x}S$ nanocrystals: optical and structural properties of copper-deficient copper(I) sulfides. J Am Chem Soc 131:4253–4261

[26] Lukashev P, Lambrecht WRL, Kotani T, van Schilfgaarde M (2007) Electronic and crystal structure of $Cu_{2-x}S$: full-potential electronic structure calculations. Phys Rev B Condens Matter Mater Phys 76:195202

[27] Chen HJ, Kou XS, Yang Z, Ni WH, Wang JF (2008) Shape- and size-dependent refractive index sensitivity of gold nanoparticles. Langmuir 24:5233–5237

[28] Simon T, Bouchonville N, Berr MJ, Vaneski A, Adrovic A, Volbers D, Wyrwich R, Döblinger M, Susha AS, Rogach AL, Jäckel F, Stolarczyk JK, Feldmann J (2014) Redox shuttle mechanism enhances photocatalytic H_2 generation on Ni-decorated CdS nanorods. Nat Mater 13:1013–1018

[29] Jain PK, Manthiram K, Engel JH, White SL, Faucheaux JA, Alivisatos AP (2013) Doped nanocrystals as plasmonic probes of redox chemistry. Angew Chem Int Ed 52:13671–13675

[30] Nørby P, Johnsen S, Iversen BB (2014) In Situ X-ray diffraction study of the formation, growth, and phase transition of colloidal $Cu_{2-x}S$ nanocrystals. ACS Nano 8:4295–4303

[31] Liu Y, Liu MX, Swihart MT (2017) Reversible crystal phase interconversion between covellite CuS and high chalcocite Cu_2S nanocrystals. Chem Mater 29:4783–4791

[32] Wang FF, Li Q, Lin L, Peng HL, Liu ZF, Xu DS (2015) Monodisperse copper chalcogenide nanocrystals: controllable synthesis and the pinning of plasmonic resonance absorption. J Am Chem Soc 137:12006–12012

[33] Sheikholeslami S, Jun YW, Jain PK, Alivisatos AP (2010) Coupling of optical resonances in a compositionally asymmetric plasmonic nanoparticle dimer. Nano Lett 10:2655–2660

[34] Jain PK, El-Sayed MA (2010) Plasmonic coupling in noble metal nanostructures. Chem Phys Lett 487:153–164

[35] Chen LH, Li GH (2018) Functions of 1-dodecanethiol in the synthesis and post-treatment of copper sulfide nanoparticles relevant to their photocatalytic applications. ACS Appl Nano Mater 1:4587–4593

[36] Kriegel I, Rodríguez-Fernández J, da Como E, Lutich AA, Szeifert JM, Feldmann J (2011) Tuning the light absorption of $Cu_{1.97}S$ nanocrystals in supercrystal structures. Chem Mater 23:1830–1834

[37] Furube A, Yoshinaga T, Kanehara M, Eguchi M, Teranishi T (2012) Electric-field enhancement inducing near-infrared two-photon absorption in an indium-tin oxide nanoparticle film. Angew Chem Int Ed 51:2640–2642